Journal of Solid State Chemistry 181 (2008) 3248–3256

Contents lists available at ScienceDirect

Journal of Solid State Chemistry

journal homepage: www.elsevier.com/locate/jssc

Controlled synthesis of nanocrystalline CeO_2 and $Ce_{1-x}M_xO_{2-\delta}$ (M = Zr, Y, Ti, Pr and Fe) solid solutions by the hydrothermal method: Structure and oxygen storage capacity

Preetam Singh, M.S. Hegde *

Solid State and Structural Chemistry Unit, Indian Institute of Science, Bangalore 560012, India

ARTICLE INFO

Article history:
Received 9 July 2008
Received in revised form
5 August 2008
Accepted 9 August 2008
Available online 22 August 2008

Keywords:
Ceria
Nanocrystallites
Hydrothermal synthesis
Oxygen storage capacity
CO oxidation

ABSTRACT

CeO_2 and $Ce_{1-x}M_xO_{2-\delta}$ (M = Zr, Ti, Pr, Y and Fe) nanocrystallites of 5–10 nm sizes have been synthesized by hydrothermal method using diethylenetriamine (DETA) and melamine as complexing agents. Compounds have been characterized by powder X-ray diffraction (XRD), transmission electron microscopy (TEM), X-ray photoelectron spectroscopy (XPS) and energy dispersive X-ray analysis (EDX) and their structures have been refined by the Rietveld method. All the compounds crystallize in cubic fluorite structure. Even up to 50% Zr and Y, 40% Ti, 25% Pr and 15% Fe is substituted for Ce^{4+} in CeO_2 by this method. Sizes of crystallites can be tuned by changing the complexing agent and reaction temperature. Nanocrystalline CeO_2 and $Ce_{1-x}Zr_xO_2$ prepared here have higher or at least competitive oxygen storage capacity (OSC) than those reported in literature. $Ce_{1-x}Fe_xO_{2-\delta}$ shows higher OSC and higher percentage of CO oxidation at lower temperature than $Ce_{1-x}Zr_xO_2$.

1. Introduction

Controlled synthesis of inorganic nanoparticles has become one of the important areas of materials chemistry because of their size- and shape-dependent properties and their potential of self-assembly as building blocks and mesocrystals [1,2]. Ceria (CeO_2) is one of the most reactive rare-earth oxides and it has attracted a great deal of attention due to its unique application in catalysis, fuel cells, solar cells, gates for metal oxide, semiconductor devices and phosphor [3–7]. CeO_2 is known to release a high proportion of its oxygen for CO oxidation while retaining its fluorite structure. Amount of lattice oxygen that can be reversibly exchanged from CeO_2 is called oxygen storage capacity (OSC). Reducibility of CeO_2 to the extent of utilization of surface oxygen is dependent on the size of nanocrystallites: smaller the crystallite size, higher the reducibility. Electronic and catalytic properties of CeO_2 can be modified by isovalent and aliovalant metal ion substitution in CeO_2, provided its fluorite structure is retained with higher thermal stability.

Even though ZrO_2 cannot be reduced by H_2 or CO, $Ce_{1-x}Zr_xO_2$ shows higher reducibility than CeO_2. Therefore, synthesis of nanocrystalline $Ce_{1-x}M_xO_2$ is important. Ti, Hf and transition metal ion substitution in CeO_2 can also enhance the reducibility of CeO_2. $Ce_{1-x}M_xO_2$ (M = Zr, Hf and Ti) have been synthesized by solution combustion method but sizes of crystallites are in the 20–40 nm range [8,9]. Hydrothermal method has been employed to synthesize CeO_2 and $Ce_{1-x}M_xO_{2-\delta}$ (M = La, Pr, Ca, Sm and Bi) using NH_4OH and NaOH [10–16]. Only about 10% Fe ion could be substituted in CeO_2 by low-temperature method using NaOH [17]. Crystallite sizes are in the range of 35–50 nm and these lower valant metal ion-substituted CeO_2 were made to study oxide ion conductivity only and redox properties of Ce^{4+} have not been studied.

Here, we report hydrothermal synthesis of CeO_2 and $Ce_{1-x}M_xO_{2-\delta}$ (M = Zr, Ti, Pr, Y and Fe) nanocrystallites with new ligands like diethylenetriamine (DETA) and melamine. Sizes of crystallites are in the 4–12 nm range, which can be tuned by varying the temperature and time of the reaction. To see the effect of metal ions substitution in CeO_2, we have studied redox properties by measuring OSC of $Ce_{1-x}M_xO_{2-\delta}$ nanocrystallites. Lattice oxygen from $Ce_{1-x}Fe_xO_{2-\delta}$ is utilized by CO or H_2 at lower temperature than $Ce_{1-x}Zr_xO_2$.

2. Experimental

In total, 2.5 mM of ceric ammonium nitrate, $Ce(NH_4)_2(NO_3)_6$ (CAN) was dissolved in 45 mL of water and 7.5 mM of melamine ($C_3N_6H_6$) or DETA ($H_2NCH_2CH_2NHCH_2CH_2NH_2$) was added. The resulting gel was stirred for 10 min. There is no change in the

* Corresponding author. Fax: +91 080 2360 1310.
E-mail address: mshegde@sscu.iisc.ernet.in (M.S. Hegde).

0022-4596/$ - see front matter © 2008 Elsevier Inc. All rights reserved.
doi:10.1016/j.jssc.2008.08.018

Table 1
Composition and synthesis condition of $Ce_{1-x}M_xO_{2-\delta}$

Compound	Metal salts (M) and temperature (°C)	Complexing agent (CA)	Molar ratio CAN:M:CA	Composition
CeO_2	CAN (150 and 200 °C)	Melamine	1:0:2	CeO_2
	CAN (150 and 200 °C)	DETA	1:0:3	
$Ce_{1-x}Zr_xO_2$	CAN, $Zr(NO_3)_4$ (200 °C)	Melamine	$1-x:x:2$	$x = 0.25, 0.50$
$Ce_{1-x}Ti_xO_2$	CAN, $TiO(NO_3)_2$ from titanium isopropoxide (200 °C)	DETA	$1-x:x:3$	$x = 0.25, 0.40$
$Ce_{1-x}Fe_xO_{2-\delta}$	CAN, $Fe(NO_3)_3$ (200 °C)	DETA	$1-x:x:3$	$x = 0.05, 0.10$ and 0.15
$Ce_{1-x}Y_xO_{2-\delta}$[a]	CAN, (Y_2O_3+HNO_3) (200 °C)	DETA	$1-x:x:3$	$x = 0.10, 0.30$ and 0.50
$Ce_{1-x}Pr_xO_{2-\delta}$[a]	CAN, (Pr_6O_{11}+HNO_3) (200 °C)	DETA	$1-x:x:3$	$x = 0.10$ and 0.25

[a] Y_2O_3 and Pr_6O_{11} are dissolved in minimum amount of dilute HNO_3, evaporated to dryness and redissolved in water.

orange color of CAN solution when DETA or melamine is added; the solution turned into a gel. The gel was transferred to three autoclave bombs of 20 mL capacity with 75% of filling and they were placed in hot air oven at 200 °C for 24 h. The crystalline solid obtained was filtered and dried in hot air oven at 100 °C for 5 h. To study the effect of reaction temperature and time, synthesis was carried out at 150 and 200 °C for 12 or 24 h. CeO_2 was also prepared with NaOH under similar condition. Ratio of metal salts and ligands are very important for synthesis CeO_2 nanocrystallites. When molar ratio of metal to DETA was 1:2, yield was very low but when ratio was 1:3, 100% yield is obtained. Yield was 100% with melamine with 1:2 ratio of metal to melamine. $Ce_{1-x}M_xO_{2-\delta}$ (M = Zr, Y, Ti, Pr and Fe) were synthesized by taking CAN and metal salt in required molar ratio with DETA or melamine. Several complexing agents were tried to make CeO_2 in a single step. Even though CeO_2 can be prepared by urea hydrolysis at 100 °C, in hydrothermal condition $Ce(OH)CO_3$ was formed [18]. Glycine and ethylene glycol also gave Ce–ligand complexes instead of CeO_2. However with DETA and melamine CeO_2 is precipitated directly. Details of preparation condition are given in Table 1.

X-ray diffraction patterns of all samples were recorded in a Phillips X'Pert diffractometer using Cu$K\alpha$ radiation at scan rate of 0.25°/min with 0.01° step size in the 2θ range between 10° and 80°. Cu$K\beta$ radiations were filtered with a graphite crystal post monochromator. Structures were refined by the Rietveld method, using FullProf-fp2k program [19].

For transmission electron microscopy (TEM), toluene dispersion of the sample was dropped onto the holey carbon-coated Cu grids, and the grids were allowed to dry in the air. The grids were examined with FEI Technai 20 at 200 kV. X-ray photoelectron spectroscopy (XPS) of selected samples was recorded in Thermo Scientific Multilab 2000 instrument. Binding energies are accurate within ±0.1 eV.

To study the redox properties of CeO_2 and $Ce_{1-x}M_xO_{2-\delta}$, hydrogen uptake measurements were performed in a microreactor of length 30 cm and internal diameter (0.4 cm) with 5.49% H_2/Ar (certified calibration gas mixture from Bhoruka gases Ltd., India) flowing at 30 sccm at a linear heating rate of 5 °C/min up to 600 °C. Volume of hydrogen uptake was calibrated against CuO.

3. Results and discussion

3.1. CeO_2

The powder X-ray diffraction patterns of as-prepared compounds with DETA or melamine at different temperatures are shown in Fig. 1. The pattern is indexed to fluorite CeO_2 structure and diffraction lines due to any of Ce–ligand complex are not observed. CeO_2 is obtained directly with these two ligands and yield is quantitative. X-ray diffraction (XRD) pattern of CeO_2 made with NaOH in similar condition is also given in Fig. 1 for comparison. Diffraction lines of CeO_2 made with melamine and DETA are much broader compared with CeO_2 made with NaOH. Diffraction lines for CeO_2 with melamine at 150 °C are much broader compared with CeO_2 with DETA at 150°C. Rietveld refined XRD profiles of CeO_2 made with melamine at 150 °C and CeO_2 made with DETA at 200 °C are shown in Fig. 2. The background of XRD pattern is flat clearly demonstrating that the material is crystalline. The refined X-ray profiles fit well with the observed X-ray data. Crystallite sizes were estimated following Scherrer formula [20]:

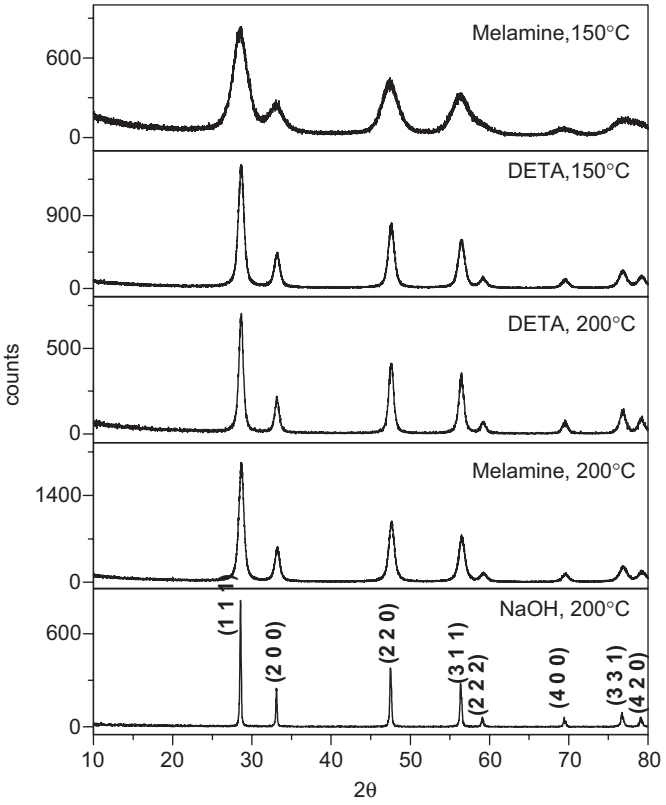

Fig. 1. XRD pattern of as-prepared CeO_2 with different ligands and temperatures.

$$\text{Crystallites size (d)} = 0.9\lambda/\beta\cos\theta \quad (1)$$

where λ is the wavelength of X-ray, β the full width at half maxima (FWHM) in radian and θ the diffraction angle. FWHM was estimated taking the U, V, W values from the Rietveld refinement data given by the equation [21]

$$\beta = (U\tan^2\theta + V\tan\theta + W)^{1/2} \quad (2)$$

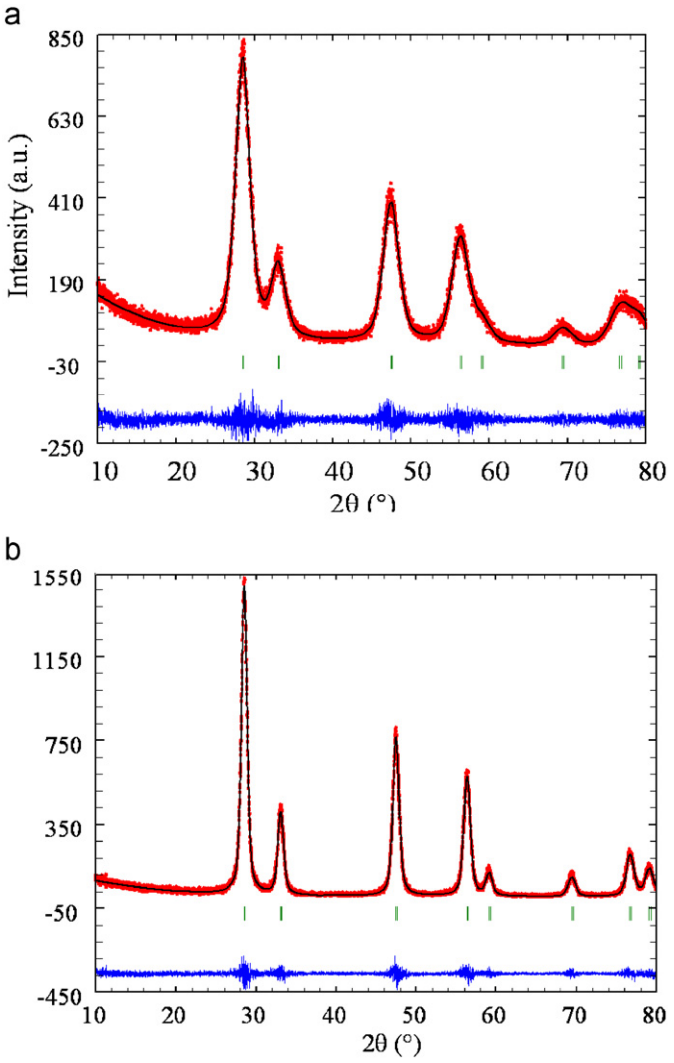

Fig. 2. The Rietveld refined XRD profile of CeO_2 (a) with melamine at 150 °C and (b) with DETA at 200 °C.

where β values were also obtained by direct measurement of FWHM from the (111), (200), (220) and (311) diffraction lines. Crystallite size obtained by both the methods along with lattice parameter, R_f, R_{bragg}, χ^2 are summarized in Table 2. Crystallite sizes obtained from the β values from Eq. (2), agree well with β values obtained from the direct measurements of X-ray diffraction lines as can be seen from Table 2. Lattice parameter, a, of CeO_2 is 5.411 A (JCPDS No. 340394). The lattice parameter 'a' of the nanocrystalline CeO_2 is slightly higher than sintered CeO_2 and a values agree well with literature values correspond to nanocrystalline CeO_2 [22]. Average crystallite size of CeO_2 obtained with NaOH is in 51 nm while with melamine and DETA, sizes are in the 4–12 nm range under similar experimental condition.

HRTEM image, bright field image and electron diffraction pattern of CeO_2 made with melamine at different temperatures are shown in Fig. 3(a) and (b). Average crystallite size of CeO_2 made with melamine at 150 °C is 5 nm and melamine at 200 °C is 8 nm. Average crystallites size for CeO_2 made with DETA at 200 °C is around 10 nm. The crystallite sizes obtained from TEM given in Table 2 agree well with those obtained from the X-ray line broadening. Electron diffraction pattern from these crystallites is indexed to fluorite structure of CeO_2. Thus, CeO_2 of 4–5 nm sizes can be made by the hydrothermal synthesis with melamine.

UV absorption spectra of nanocrystalline CeO_2 made with complexing agents at different temperature are shown in Fig. 4. CeO_2 made with NaOH, DETA and melamine at 200 and 150 °C shows absorption edges at 610, 495, 470 and 445 nm, respectively. Highly crystalline CeO_2 shows absorption edge at 610 nm with a band gap of 2.03 eV. Blue shift is due to decrease in sizes of CeO_2. Band gap increased from 2.03 to 2.78 eV with decrease in size of CeO_2 from 50 to 5 nm. The absorption of CeO_2 in the UV–visible region originates from the charge transfer transition from O ($2p$) to Ce ($4f$) [22–24].

Having made different sizes of CeO_2, OSC were measured. H_2/TPR profiles of CeO_2 of different sizes are shown in Fig. 5(a) and (b). CeO_2 made with melamine at 200 °C can be reduced to $CeO_{1.96}$ which is equivalent to 2.6 cc/g of [O]. But CeO_2 made with melamine at 150 °C can be reduced to $CeO_{1.86}$ which is equivalent to 10.4 cc/g of [O]. Thus, smaller the size of nanocrystallites, higher is the reducibility and OSC.

Table 2
Structural parameters of CeO_2 and $Ce_{1-x}M_xO_{2-\delta}$ (M = Zr, Ti, Pr, Y and Fe) made with different complexing agents

Compound	Lattice parameter (Å)	R_f	R_{bragg}	χ^2	Size from XRD-plot (nm)	Size from the Rietveld refinement (nm)	Actual size from TEM (nm)
CeO_2 with NaOH, 150 °C	5.4147 (6)	3.39	3.90	1.19	51.5±0.2	51.5	
CeO_2 with DETA, 200 °C	5.4156 (7)	3.12	2.38	1.16	12.0±0.1	12.1	10±2
CeO_2 with DETA, 150 °C	5.4130 (7)	1.21	1.47	1.28	9.7±0.1	9.7	10±2
CeO_2 with melamine, 200 °C	5.4135 (13)	1.29	1.08	1.17	10.9±0.1	10.9	8±1
CeO_2 with melamine, 150 °C	5.4164 (12)	1.35	0.932	1.10	3.7±0.2	3.8	5±1
$Ce_{0.75}Zr_{0.25}O_2$	5.3437 (9)	3.21	4.20	1.13	10.0	10.1	
$Ce_{0.50}Zr_{0.50}O_2$	5.2714 (2)	3.19	4.78	1.10	7.1	7.2	
$Ce_{0.75}Ti_{0.25}O_2$	5.3975(7)	1.53	2.29	0.85	10.2	10.2	
$Ce_{0.60}Ti_{0.40}O_2$	5.3425 (2)	2.00	2.56	0.76	7.5	7.7	9±1
$Ce_{0.90}Pr_{0.10}O_{2-\delta}$	5.4307 (5)	1.24	1.46	0.90	10.9	11.0	
$Ce_{0.75}Pr_{0.25}O_{2-\delta}$	5.4461 (5)	1.55	2.11	1.01	7.0	7.1	8±1
$Ce_{0.90}Y_{0.10}O_{1.95}$	5.4151 (5)	1.12	1.58	0.90	8.6	8.7	
$Ce_{0.70}Y_{0.30}O_{1.85}$	5.4104 (1)	0.76	0.84	0.75	6.0	6.2	
$Ce_{0.50}Y_{0.50}O_{1.75}$	5.3854 (2)	0.65	0.87	0.85	4.9	5.2	6±1
$Ce_{0.95}Fe_{0.05}O_{1.95}$	5.4084 (5)	0.6	1.38	0.97	8.3	8.0	
$Ce_{0.90}Fe_{0.10}O_{1.90}$	5.4062 (7)	0.61	0.96	1.14	8.3	8.0	
$Ce_{0.85}Fe_{0.15}O_{1.85}$	5.4036 (1)	1.20	1.92	0.92	10.7	11.3	10±2

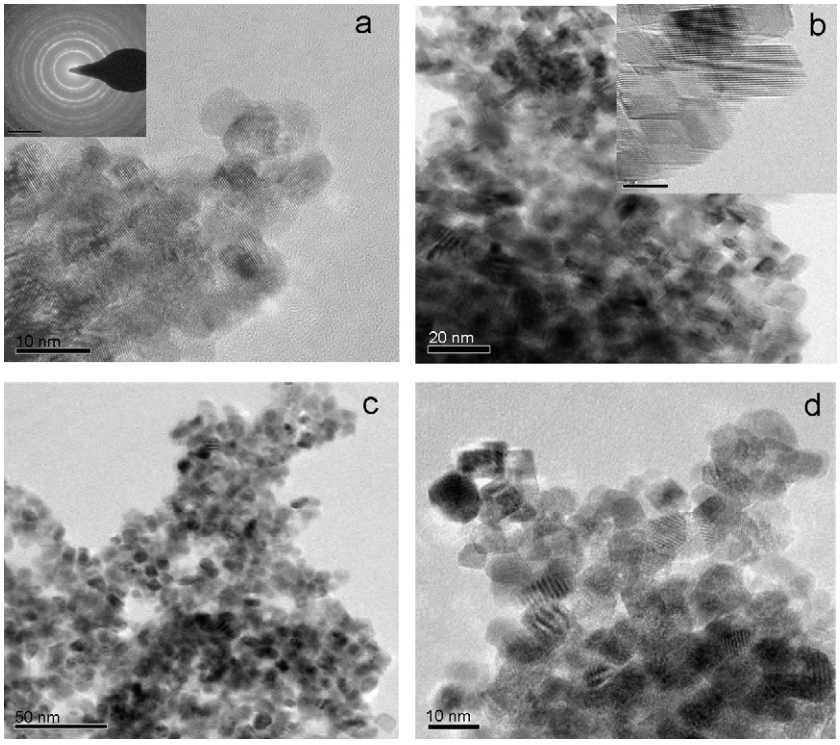

Fig. 3. (a) HRTEM image and electron diffraction of CeO_2 with melamine at 150 °C, (b) bright field image and HRTEM of CeO_2 with melamine at 200 °C and (c, d) bright and HRTEM images of $Ce_{0.75}Pr_{0.25}O_{2-\delta}$.

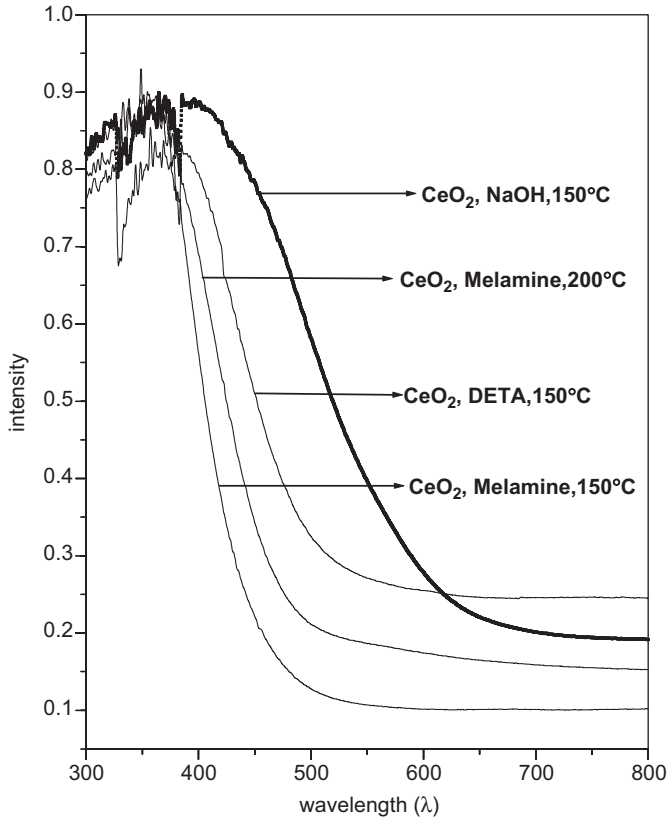

Fig. 4. UV–visible absorption spectra of CeO_2 made with different complexing agent at different temperature and made with NaOH.

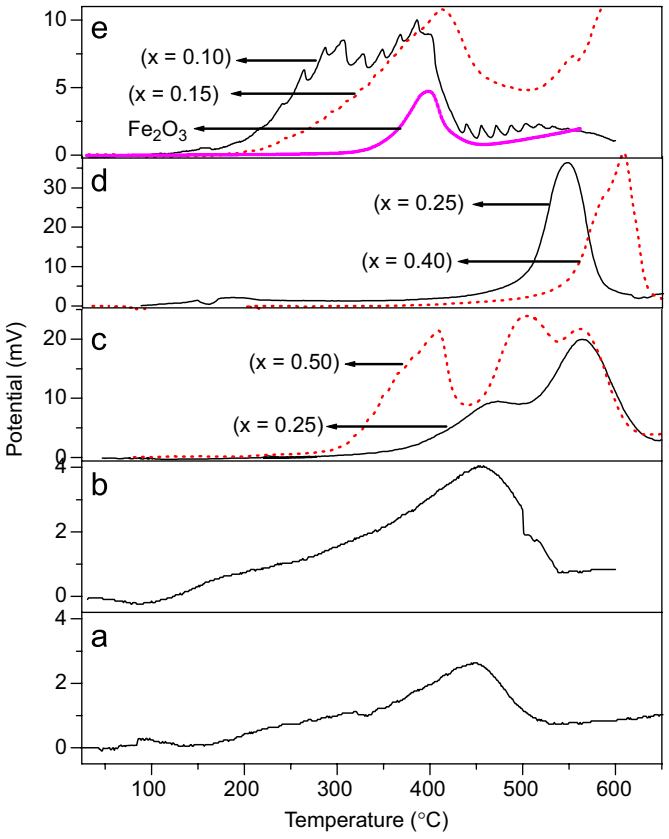

Fig. 5. Hydrogen uptake plot of (a) CeO_2 (8–10 nm), (b) CeO_2 (4–5 nm), (c) $Ce_{1-x}Zr_xO_2$ ($x = 0.25$ and 0.50), (d) $Ce_{1-x}Ti_xO_2$ ($x = 0.25$ and 0.40) and (e) $Ce_{1-x}Fe_xO_{2-\delta}$ ($x = 0.10$ and $= 0.15$) and Fe_2O_3.

Hydrothermal synthesis route is employed here to synthesize a large number of metal ion-substituted nanocrystalline CeO_2. $Ce_{1-x}M_xO_{2-\delta}$ (M = Zr, Y, Ti, Pr and Fe) nanocrystallites are synthesized with DETA and melamine as a complexing agents. These ligands are forming complexes with metal ion in the form of a gel and in the hydrothermal condition slow base hydrolysis results in the formation of oxide nanocrystallites. A mechanism for formation of nanocrystallites is given below:

$$Ce(NH_4)_2(NO_3)_6 \cdot 6H_2O + 3NH_2CH_2CH_2NHCH_2CH_2NH_2$$
$$\downarrow$$
$$(Gel) \Rightarrow Ce(NH_4)_2(NH_2CH_2CH_2NHCH_2CH_2NH_2)_3(NO_3)_6 + 6H_2O$$
$$(Hydrolysis) NH_2CH_2CH_2NHCH_2CH_2NH_2 + 3H_2O \rightarrow 2NH_2CH_2CH_2OH + NH_4OH$$
$$NH_4OH \Leftrightarrow NH_4^+ + OH^-$$
$$Ce_4^+ + 4OH^- \rightarrow CeO_2 + 2H_2O$$

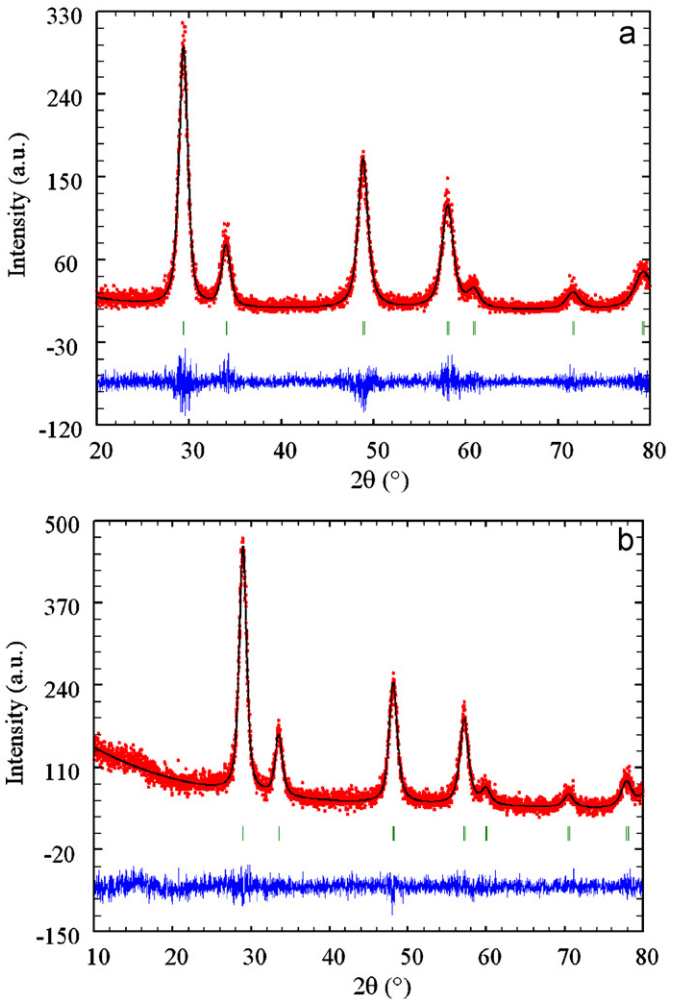

Fig. 6. The Rietveld refined X-ray profile of (a) $Ce_{0.50}Zr_{0.50}O_2$ and (b) $Ce_{0.60}Ti_{0.40}O_2$.

pH of the gel was 7.5–8 with DETA and was ~7 with melamine means slower hydrolysis occurs with melamine, which results slower growth rate of CeO_2. Thus, smaller size crystallites are formed with melamine. Melamine is soluble in hot water; $TiO(NO_3)_2$ in hot water hydrolyzes into TiO_2. Therefore, melamine could not be used for the preparation of $Ce_{1-x}Ti_xO_2$. $Ce_{1-x}Zr_xO_2$ ($x = 0.25$ and 0.50) nanocrystallites form only with melamine as a complexing agent. When DETA is used for synthesis of $Ce_{1-x}Zr_xO_2$, ZrO_2 separated out possibly due to faster hydrolysis of Zr–DETA complex. This is confirmed by the synthesis of ZrO_2 (monoclinic) with DETA. DETA forms complexes with most of metal salts. That is why we have used DETA in most of cases and $Ce_{1-x}M_xO_{2-\delta}$ (M = Y, Ti, Pr and Fe) nanocrystallites solid solutions were synthesized using DETA as a complexing agent.

3.2. $Ce_{1-x}Zr_xO_2$

$Ce_{1-x}Zr_xO_2$ ($0 \leqslant x \leqslant 0.5$) could be synthesized only with melamine and not with DETA. The Rietveld refined X-ray diffraction pattern of $Ce_{0.50}Zr_{0.50}O_2$ is shown in Fig. 6(a) and it crystallizes in $Fm3m$ space group of cubic fluorite lattice. Structural data of $Ce_{1-x}Zr_xO_2$ ($x = 0.25$ and 0.50) obtained by the Rietveld refinement from powder XRD data are summarized in Table 2. Crystallite sizes are in the range of 7–10 nm. Lattice parameters agree well with literature value [25].

Hydrogen uptake measurements were carried out for $Ce_{1-x}Zr_xO_2$ ($x = 0.25$ and 0.50) samples. A H_2 TPR profile of $Ce_{1-x}Zr_xO_2$ ($x = 0.25$ and 0.50) are shown in Fig. 5(c). $Ce_{0.75}Zr_{0.25}O_2$ reduced from $Ce_{0.75}Zr_{0.25}O_2$ to $Ce_{0.75}Zr_{0.25}O_{1.84}$ which is equivalent to 22.41 cc/g. Note that the Y scale in Fig. 5 is different in each case. Hydrogen uptake measurements are up to 650 °C and total OSC up to 650 °C are given in Table 3. O_2 is passed while cooling from 650 °C and H_2 uptake is fully reversible. It is important to note that $Ce_{0.50}Zr_{0.50}O_2$ made here is of 7–10 nm sizes and the compound could be reduced to $Ce_{0.50}Zr_{0.50}O_{1.64}$. Normally, $Ce_{0.50}Zr_{0.50}O_2$ cannot be reduced beyond $Ce_{0.50}Zr_{0.50}O_{1.75}$ and if

Table 3
Composition of metal substituted CeO_2 before and after H_2 uptake and OSC value up to 600 °C

Compound	Composition		Oxygen storage capacity (cc/g)
	Before reduction	After reduction	
CeO_2	CeO_2 (10 nm)	$Ce^{4+}_{0.94}Ce^{3+}_{0.06}O_{1.97}$	3.9
	CeO_2 (5 nm)	$Ce^{4+}_{0.84}Ce^{3+}_{0.16}O_{1.92}$	10.4
$Ce_{1-x}Zr_xO_2$	$Ce^{4+}_{0.75}Zr^{4+}_{0.25}O_2$	$Ce^{4+}_{0.43}Ce^{3+}_{0.32}Zr^{4+}_{0.25}O_{1.84}$	22.4
	$Ce^{4+}_{0.50}Zr^{4+}_{0.50}O_2$	$Ce_{0.50}Zr_{0.50}O_{1.64}$	54.6
$Ce_{1-x}Ti_xO_2$	$Ce^{4+}_{0.75}Ti^{4+}_{0.25}O_2$	$Ce_{0.75}Ti_{0.25}O_{1.86}$	21.0
	$Ce^{4+}_{0.60}Ti^{4+}_{0.40}O_2$	$Ce_{0.60}Ti_{0.40}O_{1.84}$	27.3
$Ce_{1-x}Pr_xO_{2-x/2}$	$Ce^{4+}_{0.90}Pr^{3+}_{0.10}O_{1.95}$	$Ce^{4+}_{0.60}Ce^{3+}_{0.30}Pr^{3+}_{0.10}O_{1.80}$	19.6
	$Ce^{4+}_{0.75}Pr^{3+}_{0.25}O_{1.875}$	$Ce^{4+}_{0.59}Ce^{3+}_{0.16}Pr^{3+}_{0.25}O_{1.795}$	11.0
$Ce_{1-x}Y_xO_{2-x/2}$	$Ce^{4+}_{070}Y^{3+}_{0.30}O_{1.85}$	$Ce^{4+}_{0.58}Ce^{3+}_{0.12}Y^{3+}_{0.30}O_{1.79}$	8.5
	$Ce^{4+}_{0.50}Y^{3+}_{0.50}O_{1.75}$	$Ce^{4+}_{0.46}Ce^{3+}_{0.04}Y_{0.50}O_{1.72}$	4.5
$Ce_{1-x}Fe_xO_{2-x/2}$	$Ce^{4+}_{0.80}Ce^{3+}_{0.10}Fe^{3+}_{0.10}O_{1.90}$	$Ce^{4+}_{0.64}Ce^{3+}_{0.26}Fe^{2+}_{0.10}O_{1.76}$	18.6
	$Ce^{4+}_{0.75}Ce^{3+}_{0.15}Fe^{3+}_{0.15}O_{1.85}$	$Ce^{4+}_{0.49}Ce^{3+}_{0.36}Fe^{2+}_{0.15}O_{1.67}$	25.6

cations are ordered, it can go to $Ce_2Zr_2O_7$ pyrochlore phase with Ce in 3+ and Zr in 4+ states [26]. Here, 7–10 nm crystallites of $Ce_{0.50}Zr_{0.50}O_2$ can be reduced beyond $Ce_{0.50}Zr_{0.50}O_{1.75}$. The reduced compound is black in color and conducting in nature. Tinku et al. in this laboratory have studied H_2 reduction of $Ce_{0.50}Zr_{0.50}O_2$ prepared by solution combustion method [9]. Nanocrystalline CeO_2 and $Ce_{1-x}Zr_xO_2$ prepared here show higher or at least competitive OSC than those reported in literature [27].

3.3. $Ce_{1-x}Ti_xO_2$

Ti-substituted $Ce_{1-x}Ti_xO_2$ ($x = 0.25$ and 0.40) nanocrystallites have been synthesized with DETA as a complexing agent by hydrothermal method at 200 °C. Up to 40% of Ti can be substituted for Ce^{4+} by this method. The Rietveld refined XRD profile of $Ce_{0.60}Ti_{0.40}O_2$ is shown in Fig. 6(b). Decrease in lattice parameter of $Ce_{0.75}Ti_{0.25}O_2$ is due to substitution of lower ionic radii of Ti^{4+} (0.74 Å) compared with Ce^{4+} (0.97 Å). Structural parameters are summarized in Table 2.

HRTEM and bright field image of $Ce_{0.60}Ti_{0.40}O_2$ is shown in Figs. 7(a) and (b). Average crystallite size of $Ce_{0.60}Ti_{0.40}O_2$ is 9 nm. Sizes obtained from TEM study agree well with XRD data. Sizes of nanocrystallites can be decreased further by decreasing the reaction temperature.

Hydrogen uptake measurements were carried out for $Ce_{1-x}Ti_xO_2$ ($x = 0.25$ and 0.40) samples and their H_2/TPR profiles are shown in Fig. 5(d). $Ce_{0.75}Ti_{0.25}O_2$, reduced to $Ce_{0.75}Ti_{0.25}O_{1.86}$ which is equivalent to 21 cc/g of [O]. Similarly, $Ce_{0.60}Ti_{0.40}O_2$ reduced to $Ce_{0.60}Ti_{0.40}O_{1.84}$, which equivalent to 27.3 cc/g of [O]. Hydrogen uptake measurements were performed repeatedly by reducing in H_2 up to 650 °C and oxidizing them in O_2 and it is fully reversible.

3.4. $Ce_{1-x}Pr_xO_{2-\delta}$

$Ce_{1-x}Pr_xO_{2-\delta}$ ($x = 0.10$ and 0.25) has been synthesized with DETA as a complexing agent in hydrothermal condition. The Rietveld refined XRD profile of $Ce_{0.75}Pr_{0.25}O_{2-\delta}$ compounds made with DETA is shown in Fig. 8(a). A Core level Pr ($3d$) XPS spectra of as-prepared $Ce_{0.75}Pr_{0.25}O_{2-\delta}$ is shown in Fig. 10. Pr ($3d_{5/2}$) main peak is observed at 929.3 eV along with intense satellite peak at 933.3 eV, confirmed Pr^{3+} present in $Ce_{1-x}Pr_xO_{2-\delta}$. The compound is red in color. Increase in lattice parameters is observed due to substitution of Pr^{3+} ion ($r_i = 1.12$ Å) in CeO_2 matrix. Structural

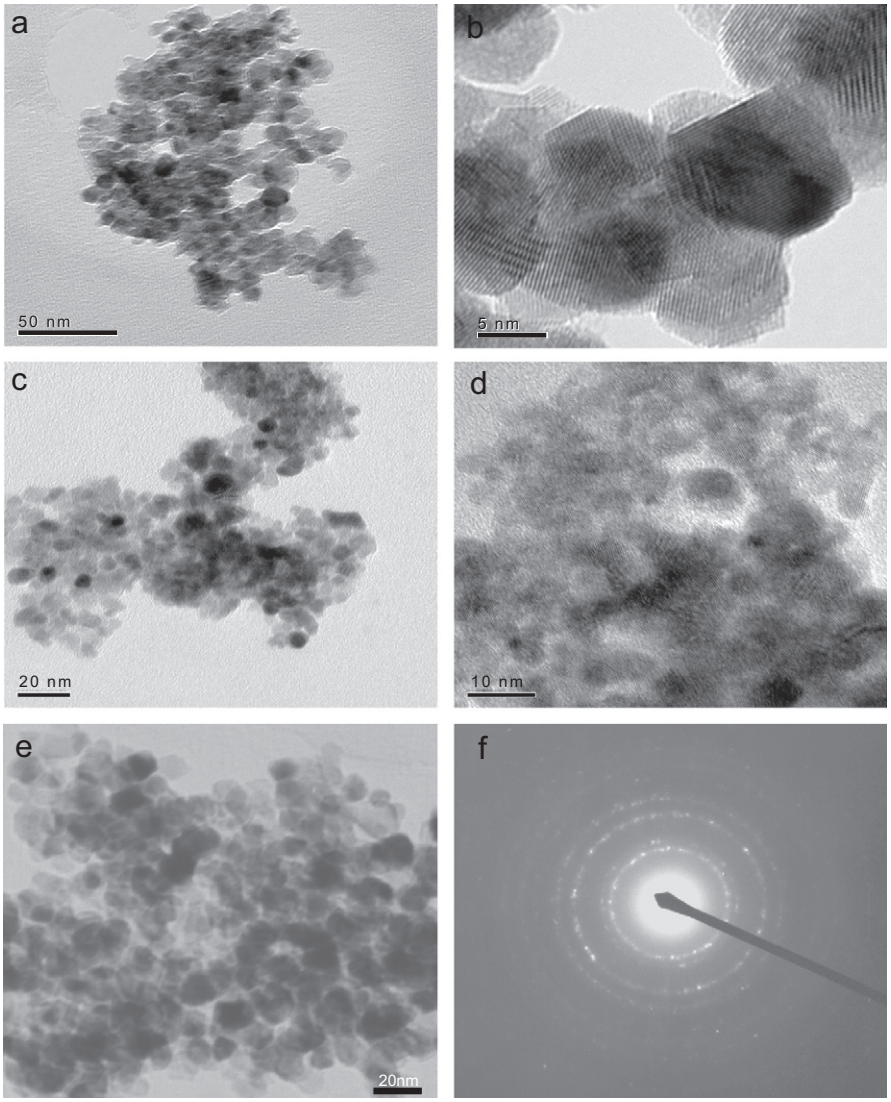

Fig. 7. (a) Bright field and (b) HRTEM image of $Ce_{0.60}Ti_{0.40}O_2$, (c) Bright field image, (d) HRTEM image of $Ce_{0.50}Y_{0.50}O_{1.75}$, (e) Bright field image and (f) ED pattern of $Ce_{0.85}Fe_{0.15}O_{2-\delta}$.

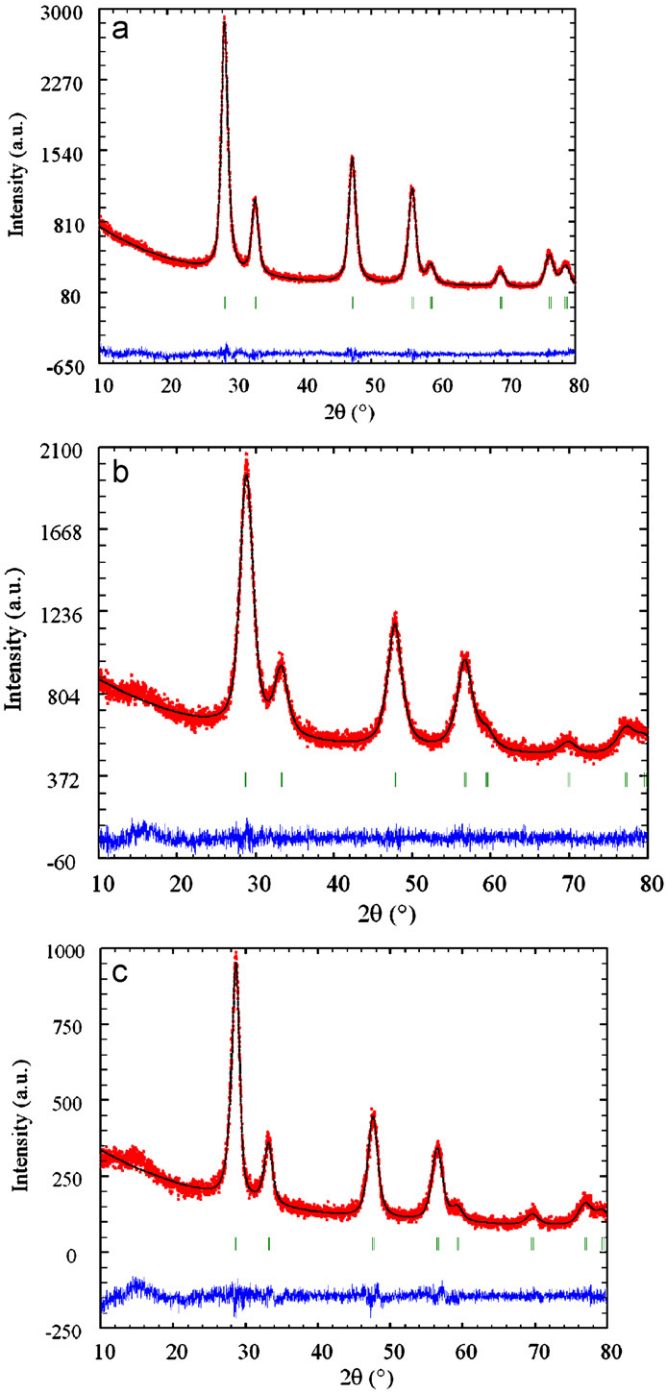

Fig. 8. The Rietveld refined XRD plot of (a) $Ce_{0.75}Pr_{0.25}O_{2-\delta}$, (b) $Ce_{0.50}Y_{0.50}O_{2-\delta}$ and (c) $Ce_{0.85}Fe_{0.15}O_{2-\delta}$.

parameters of $Ce_{1-x}Pr_xO_{2-\delta}$ ($x = 0.10$ and 0.25) obtained by the Rietveld refinement from powder XRD data are summarized in Table 2. Decrease in crystallites size is observed with increase in substitution of Pr ion in CeO_2. Bright field and HRTEM image of $Ce_{0.75}Pr_{0.25}O_{2-\delta}$ is shown in Fig. 3(c) and (d). Average crystallite size of $Ce_{0.75}Pr_{0.25}O_{2-\delta}$ is 10 nm. Sizes obtained from TEM study agree well with XRD data.

H_2 uptake study of $Ce_{0.90}Pr_{0.10}O_{1.95}$ shows reduction to $Ce_{0.90}Pr_{0.10}O_{1.80}$ which is equivalent to 19.6 cc/g of [O] and $Ce_{0.75}Pr_{0.25}O_{1.875}$ shows very little OSC of about 11 cc/g up to 600 °C. Thus, OSC value decreases with increase of Pr substitution in CeO_2. A decrease in OSC can be attributed to large amount of

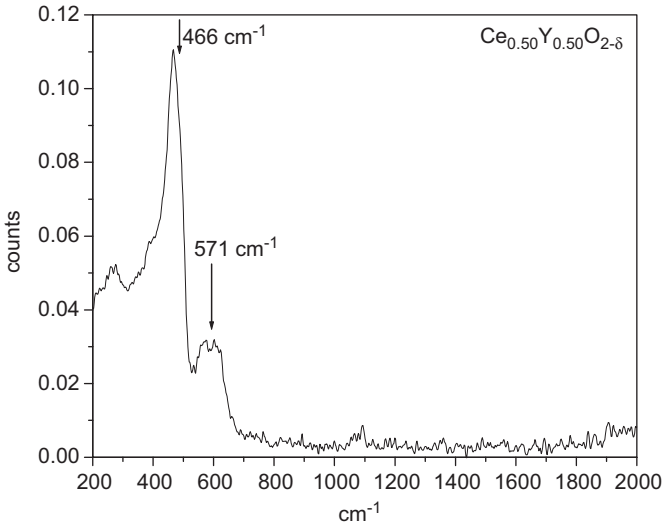

Fig. 9. Raman scattering spectra of $Ce_{0.50}Y_{0.50}O_{1.75}$.

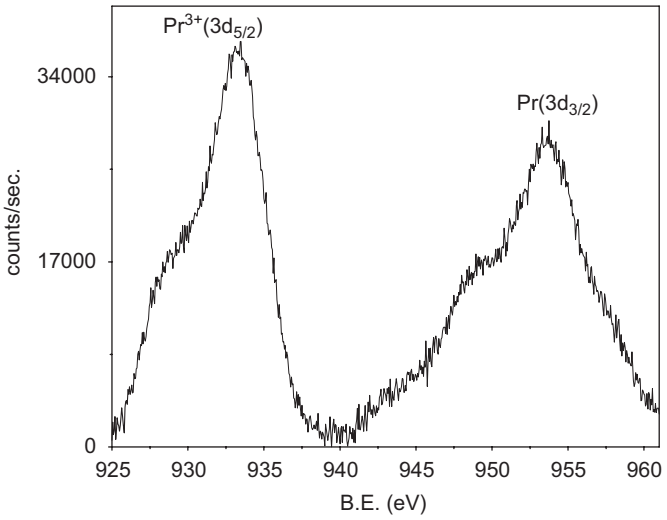

Fig. 10. XPS of Pr (3*d*) in $Ce_{0.75}Pr_{0.25}O_{1.875}$.

oxide ion vacancy created in the lattice due to Pr^{3+} ion substitution.

3.5. $Ce_{1-x}Y_xO_{2-x/2}$

$Ce_{1-x}Y_xO_{2-\delta}$ ($x = 0.10$, 0.30 and 0.50) have been synthesized with DETA as complexing agent. Up to 50% Y is substituted for Ce^{4+} in CeO_2 lattice by this method. Even with huge oxide ion vacancy, $Ce_{0.50}Y_{0.50}O_{1.75}$ crystallizes in fluorite structure. The Rietveld refined XRD profile of $Ce_{0.50}Y_{0.50}O_{1.75}$ is shown in Fig. 8(b). Lattice parameter, '*a*' of $Ce_{1-x}Y_xO_{2-x/2}$ decreases with increase in Y^{3+} substitution in CeO_2. Structural parameters of $Ce_{1-x}Y_xO_{2-x/2}$ ($x = 0.10$, 0.30 and 0.50) obtained by the Rietveld refinement from powder XRD data are summarized in Table 2.

HRTEM image and electron diffraction pattern of $Ce_{0.50}Y_{0.50}O_{1.75}$ are given in Fig. 7(c) and (d). Average crystallite size of $Ce_{0.50}Y_{0.50}O_{1.75}$ is 6 nm. Substitution and composition of yttrium is also confirmed by EDAX. Huge oxygen vacancy present in $Ce_{0.50}Y_{0.50}O_{1.75}$ is observed by Raman scattering shown in Fig. 9. High-intensity phonon mode vibration observed at 471 cm^{-1}, which is assigned to symmetric breathing mode of oxygen atoms

around cerium ions and the phonon mode scattering observed at 564 cm^{-1} is characteristic for oxygen vacancy in lattice [28].

Y^{3+} ion-substituted CeO_2 shows lower OSC and it decreases with increase in Y^{3+} content. While $Ce_{0.70}Y_{0.30}O_{1.85}$ could be reduced to $Ce_{0.70}Y_{0.30}O_{1.79}$, which is equivalent to 8.5 cc/g, $Ce_{0.50}Y_{0.50}Y_{1.75}$ could hardly be reduced. Thus, nonreducible rare-earth ion and Y^{3+} ion substitution suppresses the OSC of CeO_2.

3.6. $Ce_{1-x}Fe_xO_{2-\delta}$

There is very little attempt to substitute transition metal ions in CeO_2 lattice for OSC and other catalytic application. Even though 10% Fe^{3+} ion-substituted CeO_2 has been synthesized by Li et al. [16], redox properties of this material are not evaluated. Recently, up to 20% Fe-substituted CeO_2 have been prepared by urea hydrolysis method and best CO oxidation activity is seen with 10% of Fe ion substituted in CeO_2 [29]. We have synthesized $Ce_{1-x}Fe_xO_{2-\delta}$ ($x = 0.05$, 0.10 and 0.15) nanocrystallites with DETA as the complexing agent. The Rietveld refined XRD profile of $Ce_{0.85}Fe_{0.15}O_{2-\delta}$ compounds made with DETA is shown in Fig. 8(c). All the peaks were indexed in fluorite structure. Structural parameters of $Ce_{1-x}Fe_xO_{2-\delta}$ ($x = 0.05$, 0.10 and 0.15) obtained by the Rietveld refinement of powder XRD data are summarized in Table 2. The diffraction peak at half the angle of (111) reflection at ~14.4° is seen in the XRD pattern of $Ce_{0.60}Ti_{0.40}O_2$, $Ce_{0.75}Pr_{0.25}O_{2-\delta}$, $Ce_{0.50}Y_{0.50}O_{2-\delta}$ and $Ce_{0.85}Fe_{0.15}O_{2-\delta}$ (Figs. 6b and 8). It can be due to doubling of the lattice. But, other diffraction peaks due to doubling of the cell are not sufficiently intense as seen from the refined pattern. Therefore, further studies are needed to assign the possible super lattice formation.

Color of the compound is red indicting Fe is in 3+ state. When Fe concentration is increased to 20%, weak reflection of γ-Fe_2O_3 is seen. We believe that 17–18% of Fe can be substituted by this method. Average crystallite size of $Ce_{0.85}Fe_{0.15}O_{2-\delta}$ is 10 nm. Bright field image and diffraction pattern of $Ce_{0.85}Fe_{0.15}O_{2-\delta}$ is shown in Fig. 7(e) and (f). Sizes obtained from TEM study agree well with XRD data. Composition is confirmed by EDX analysis. Due to substitution of Fe^{3+} ($r_i = 0.69$ Å) in CeO_2 matrix, lattice parameter decreases. Decrease in lattice parameter is relatively less than expected. This is possibly due to presence of Ce^{3+}along with Ce^{4+} in $Ce_{1-x}Fe_xO_{2-\delta}$.

To study the oxidation state of Ce and Fe in $Ce_{1-x}Fe_xO_{2-\delta}$, XPS of Ce (3d) and Fe (2p) region were recorded. Core level XPS of Ce (3d) of as prepared and H_2 reduced $Ce_{0.85}Fe_{0.15}O_{2-\delta}$ and CeO_2 are shown in Fig. 11(a)–(c). Ce^{4+} ($3d_{5/2}$) peak observed at 882.7 eV along with satellite peaks at 6.4 and 16 eV below the main peak is characteristic of Ce^{4+} in CeO_2 [30]. La_2O_3, Ce_2O_3 and Pr_2O_3 shows similar Ln (3d) XPS spectra as shown for Pr^{3+}(3d) in Fig. 10. Ce_2O_3 is characterized by Ce ($3d_{5/2}$) at 883.3 eV along with an intense satellite at 887.1 eV [30]. Thus, filling of the valley between Ce^{4+}($3d_{5/2}$) at 882.7 eV and its satellite at 889.1 eV shows Ce is in mixed valant state in $Ce_{0.85}Fe_{0.15}O_{2-\delta}$. Ce(3$d$) spectrum was resolved into Ce^{3+} and Ce^{4+} components in $Ce_{0.85}Fe_{0.15}O_{2-\delta}$ and 15% of Ce is found to be in +3 state. After hydrogen reduction up to 600 °C 30% of Ce is found in +3 state. Fe ($2p_{3/2,\,1/2}$) core level XPS of as prepared and hydrogen reduced $Ce_{0.85}Fe_{0.15}O_{2-\delta}$ are shown in Fig. 12(a) and (b). Fe ($2p_{3/2}$) is at 710.3 eV and a weak satellite at 8 eV below the main peak in the as-prepared $Ce_{0.85}Fe_{0.15}O_{2-\delta}$ confirms that Fe is in +3 state. Thus, the formula of as-prepared 15% Fe-substituted CeO_2 can be given as $Ce^{4+}_{0.70}\,Ce^{3+}_{0.15}Fe^{3+}_{0.15}O_{1.85}$. Fe ($2p_{3/2}$) at 709.6 eV and satellite peak at 5 eV below the main peak confirms that Fe is in +2 states in hydrogen reduced $Ce_{0.85}Fe_{0.15}O_{2-\delta}$ [31]. It is important to note that Fe^{3+} is fully reduced to Fe^{2+} state not to Fe^0 after hydrogen reduction up to 600 °C.

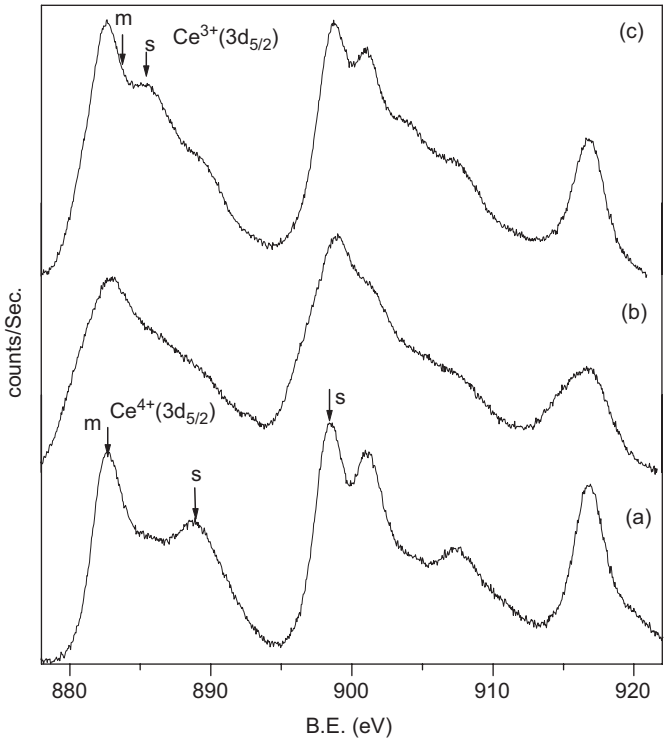

Fig. 11. XPS of Ce (3d) in (a) pure CeO_2 (b) as prepared and (c) hydrogen reduced $Ce_{0.85}Fe_{0.15}O_{2-\delta}$.

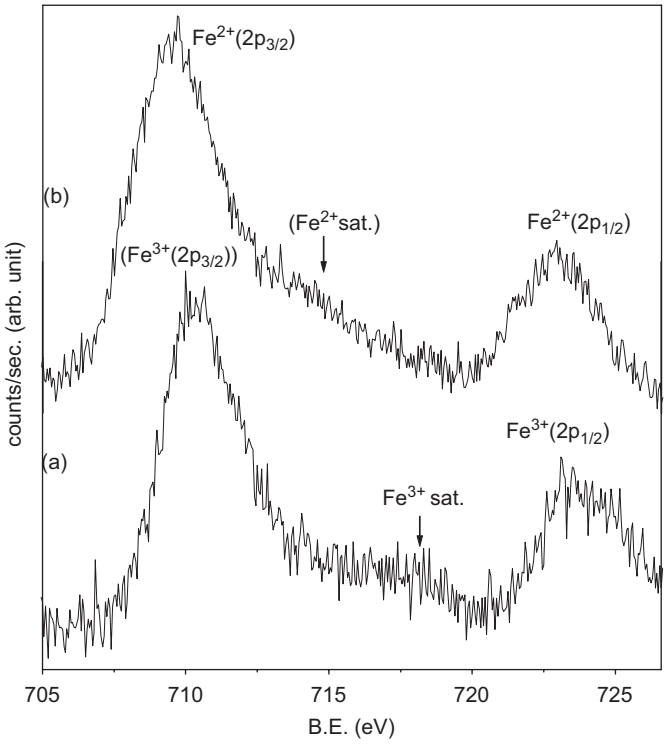

Fig. 12. XPS of Fe (2p) (a) as-prepared and (b) hydrogen reduced $Ce_{0.85}Fe_{0.15}O_{2-\delta}$.

H_2/TPR profile of $Ce_{1-x}Fe_xO_{2-\delta}$ ($x = 0.10$ and 0.15) and equivalent amount of Fe_2O_3 up to 600 °C are shown in Fig. 5(e). Peak temperature of H_2 reduction of Fe_2O_3 is 400 °C and reduction

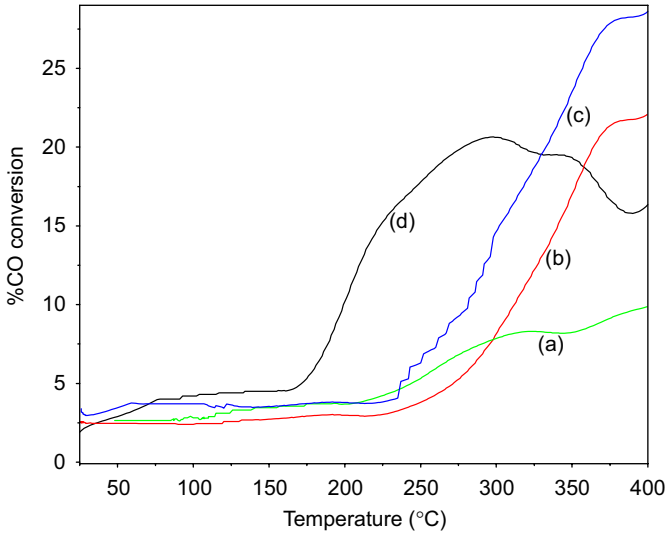

Fig. 13. The %CO conversion with lattice oxygen from (a) CeO_2 (5 nm), (b) $Ce_{0.75}Zr_{0.25}O_2$, (c) $Ce_{0.50}Zr_{0.50}O_2$ and (d) $Ce_{0.85}Fe_{0.15}O_{2-\delta}$.

starts at lower temperature in Fe-substituted CeO_2 than Fe_2O_3. Fe_2O_3 is reduced to $Fe_2O_{2.5}$ up to 600 °C. This means all of Fe^{3+} is not reduced to Fe^{+2} state. Reduction temperature of $Ce_{1-x}Fe_xO_{2-\delta}$ is lower than $Ce_{1-x}M_xO_2$ (M = Zr and Ti). $Ce_{0.90}Fe_{0.10}O_{1.90}$ can be reduced to $Ce_{0.90}Fe_{0.10}O_{1.76}$, which is equivalent to 18.5 cc/g of [O] and $Ce_{0.85}Fe_{0.15}O_{1.85}$ is reduced to $Ce_{0.85}Fe_{0.15}O_{1.67}$, which is equivalent to 25.6 cc/g. Thus, even at 15% Fe^{3+} ion substitution in CeO_2, OSC is higher than $Ce_{0.75}Zr_{0.25}O_2$. This is because Fe^{3+} is entirely reduced to Fe^{2+} in addition to partial reduction of Ce^{4+} to Ce^{3+}. Hydrogen uptake data are summarized in Table 3. Even though Fe ions in Fe_2O_3 and FeO can be reduced to Fe^0 at higher temperatures, Fe^{3+} in $Ce_{1-x}Fe_xO_{2-\delta}$ can be reduced to Fe^{2+} state only. Hydrogen uptake was repeated for several cycles following reduction and oxidation up to 600 °C, Redox behavior is fully reversible.

Having studied the OSC of these materials by H_2/TPR, CO oxidation experiments were performed to see the utilization of lattice oxygen by CO. CO oxidations were performed in a microreactor of length 30 and 0.4 cm internal diameter with 1 vol% of CO/He with total flow 100 sccm over 250 mg of catalyst at a linear heating rate of 10 °C/min up to 500 °C. $Ce_{0.85}Fe_{0.15}O_{1.85}$ shows higher percentages of CO oxidation at lower temperature than $Ce_{0.75}Zr_{0.25}O_2$ and it is shown in Fig. 13. Thus, lattice oxygen is more labile in $Ce_{1-x}Fe_xO_{2-\delta}$ and it can be utilized as an OSC material.

4. Conclusions

Controlled synthesis of CeO_2 and $Ce_{1-x}M_xO_{2-\delta}$ (M = Zr, Ti, Pr, Y and Fe) nanocrystallites is achieved by hydrothermal synthesis route using DETA and melamine as a complexing agents. Average sizes of $Ce_{1-x}M_xO_{2-\delta}$ nanocrystallites are in the 5–12 nm range. Complexation of these metal ions (M) and Ce^{4+} with DETA or melamine and simultaneous hydrolysis in hydrothermal condition leads to formation of $Ce_{1-x}M_xO_{2-\delta}$ (M = Ti, Pr, Y and Fe) nanocrystallites. Up to 15% Fe^{3+} have been substituted in CeO_2 and it is showing higher OSC and higher percentages of CO oxidation with lattice oxygen at lower temperature than $Ce_{0.75}Zr_{0.25}O_2$.

Acknowledgments

Authors thank Department of Science and Technology, Government of India for financial support. Thanks are due to Amit Mondal of Nano centre, Indian Institute of Science Bangalore and Viswanath B. of Materials Research Centre, Indian Institute of Science Bangalore for recording TEM images.

References

[1] M. Law, D.J. Sirbuly, J.C. Johnson, J. Goldberger, R.J. Saykally, P.D. Yang, Science 305 (2004) 1269–1273.
[2] E.V. Shevehenko, D.V. Talapin, C.B. Murray, S. O'Brien, J. Am. Chem. Soc. 128 (2006) 3620–3637.
[3] A. Trovareli, Catal. Rev. Sci. Eng. 38 (1996) 439–520.
[4] E.P. Murray, T. Tsai, S.A. Barnett, Nature 400 (1999) 649–651.
[5] Q. Fu, H. Saltsbarg, M. Flytzani-Stephanopoulos, Science 301 (2003) 935–938.
[6] A. Corma, P. Atienzar, H. Gracia, J.Y. Chane-Ching, Nat. Mater. 3 (2004) 394–397.
[7] A.H. Morshed, M.E. Moussa, S.M. Bedir, R. Leonard, S.X. Iiu, N. Elmasry, Appl. Phys. Lett. 70 (1997) 1647–1649.
[8] T. Baidya, A. Gayan, M.S. Hegde, N. Ravishankar, L. Dupont, J. Phys. Chem. B 110 (2006) 5262–5272.
[9] T. Baidya, M.S. Hegde, J. Gopalakrishnan, J. Phys. Chem. B 111 (2007) 5149–5154.
[10] W-Q. Han, L. Wu, Y. Zhu, J. Am. Chem. Soc. 127 (2005) 12814–12815.
[11] S. Yang, L. Gao, J. Am. Chem. Soc. 128 (2006) 9330–9331.
[12] T. Masui, H. Hirai, R. Hamad, N. Imanka, A. Gin-Ya, T. Sakata, H. Mori, J. Mater. Chem. 13 (2003) 622–627.
[13] W. Hung, P. Shuk, M. Greenblatt, Chem. Mater. 9 (1997) 2240–2245.
[14] P. Shuk, M. Greemblatt, Solid State Ionics 116 (1999) 217–223.
[15] S. Dikmen, P. Shuk, M. Greenblatt, Solid State Ionics 126 (1999) 89–95.
[16] G. Li, Y. Mao, L. Li, M. Feng, M. Wang, X. Yao, Chem. Mater. 11 (1999) 1259–1266.
[17] G. Li, R.L. Smith, H. Inomata, J. Am. Chem. Soc. 123 (2001) 11091–11092.
[18] Z. Guo, F. Du, G. Li, Z. Cui, Inorg. Chem. 45 (2006) 4167–4169.
[19] J. Rodriguez-Carvajal, Multi-pattern Rietveld Refinement program Fullprof. 2k, version 3.30, June 2005-LLB.
[20] B.D. Cullity, Elements of X-ray Diffraction, second ed., Addison-Wesley, Reading, MA, 1978.
[21] G. Caglioti, A. Paoletti, F.P. Ricci, Nucl. Instrum. Methods 3 (1958) 223–228.
[22] Ho Chunman, C. Jimmy, K. Tszyan, C. Angelo, L. Sukyin, Chem. Mater. 17 (2005) 4514–4522.
[23] T. Murata, M. Sato, H. Yoshida, K. Morinaga, J. Non-Cryst. Solids 351 (2005) 312–322.
[24] S. Tsunekawa, J. Wang, Y. Kawazoe, A. Kasuya, J. Appl. Phys. 94 (2003) 3654–3656.
[25] G. Dutta, U.V. Waghmare, T. Baidya, M.S. Hegde, K.R. Priolkar, P.R. Sarode, Catal. Lett. 108 (2006) 165–172.
[26] J.B. Thomson, A.R. Armstrong, P.G. Bruce, J. Solid State Chem. 148 (1999) 56–62.
[27] Y. Nagai, T. Yamamoto, T. Tanaka, S. Yoshida, T. Nonaka, T. Okamoto, A. Suda, M. Sugiura, Catal. Today 74 (2002) 225–234.
[28] A. Mineshige, T. Taji, Y. Moroi, M. Kobune, S. Fujii, N. Nishi, M. Inaba, Z. Ogumi, Solid State Ionics 135 (2000) 481–485.
[29] H. Bao, X. Chen, J. Fang, Z. Jiang, W. Huang, Catal. Lett. 124 (2008).
[30] A. Kotani, H. Ogasawara, J. Electron Spectrosc. Relat. Phenom. 60 (1992) 257–299.
[31] C.N.R. RaO, D.D. Sarma, S. Vasudevan, M.S. Hegde, Proc. R. Soc. Lond. A 367 (1979) 239–252.